The Effects of Crystallization Condition on the Microstructure and Thermal Stability of Istactic Polypropylene Nucleated by β-Form Nucleating Agent

Mu Dong,[1] Zhaoxia Guo,[1] Zhiqiang Su,[2] Jian Yu[1]

[1]*Institute of Polymer Science and Engineering, Department of Chemical Engineering, School of Materials Science and Engineering, Tsinghua University, Beijing 100084, China*
[2]*Key Laboratory of Beijing City on Preparation and Processing of Novel Polymer Materials, Beijing University of Chemical Technology, Beijing 100084, China*

Received 20 May 2009; accepted 22 March 2010
DOI 10.1002/app.32487
Published online 18 August 2010 in Wiley Online Library (wileyonlinelibrary.com).

ABSTRACT: This article deals with the crystallization behaviors of original (prepared in a torque rheometer), DSC crystallization and mold crystallization (quenching and slow nonisothermal crystallization) of isotactic polypropylene (iPP) mixed with β-form nucleating agent. The microstructure and thermal stability of these samples were investigated. The wide angle X-ray diffraction (WAXD) results indicate that fast cooling is favorable for β-form iPP formation. With slower cooling rate and higher concentration of nucleating agent, the lamellar thickness and stability of crystal0s were enhanced. Polarized optical microscopy (POM) and scanning electron microscopy (SEM) both showed that rapid crystallized samples gave rise to tiny spherulites, whereas under slow crystallization condition, nucleated samples could be fully developed in the form of dendritic or transcrystalline structures, depending on the nucleating agent concentration. © 2010 Wiley Periodicals, Inc. J Appl Polym Sci 119: 1374–1382, 2011

Key words: isotactic polypropylene; β-nucleating agent; crystallization; x-ray diffraction; differential scanning calorimetry

INTRODUCTION

Isotactic polypropylene (iPP) is a useful thermoplastic polymer with a wide range of applications. It has a polymorphic composition with at least four modifications: α, β, γ, and smectic.[1–6] α-iPP is known to have a monoclinic unit-cell ($a = 6.65$ Å, $b = 20.80$ Å, $c = 6.5$ Å, $\alpha = \gamma = 90°$, $\beta = 99.8°$) with layers made of isochiral helices parallel to the *ac* plane. The helices in *c* axis projection are oriented towards the $+b$ and $-b$ directions of the unit cell. β-iPP has a highly unusual crystal structure, with a trigonal unit cell ($a = b = 11.01$ Å, $c = 6.5$ Å, $\beta = 120°$), in which three isochiral helices adopt a frustrated packing. The two α and β phases are based on the same threefolded helical conformation of the chain, which differ merely by the different azimuthal setting of one helix out of three.

Among them, the most important and widely used is the α-form, which occurs under conventional crystallization conditions. But it is the β form that has been the subject of intensive investigation because of its promising mechanical properties. For example, the impact strength and toughness of β-iPP were found to exceed those of α-iPP, which can be attributed to the peculiar lamellar morphology of β-iPP,[7] including the formation of an enlarged plastic zone as well as the strain induced β–α transition during mechanical deformation.[8–10]

As the β-iPP is a metastable phase, it can be rarely obtained in a significant amount in commercial iPP products, unless crystallization conditions are favorable for the β-phase growth.[11–14] There are several approaches for obtaining substantial amount, for instance, utilization of β-nucleating agent,[15–24] copolymerization with other monomer,[25,26] crystallization induced by shear[27] external forces, like an electric/magnetic field.[28,29]

The crystallization and melting behavior of isotactic polypropylene (iPP) are closely related to its microstructure and the external conditions when these processes occur.[30–33] The change of external conditions may result in the crystal structure with different stabilities or the appearance of other crystalline modifications.[34–36] For example, at high undercooling, the formation of the modification was accompanied by the appearance of trigonal crystalline form (β-modification).[37] The perfection of crystals decreases with increasing undercooling, when the isothermal crystallization is carried out by

Correspondence to: J. Yu (yujian03@mail.tsinghua.edu.cn).
Contract grant sponsor: National Science Foundation of China; contract grant number: 20974010.
Contract grant sponsor: Beijing New-Star Program of Science and Technology; contract grant number: 2009B10.

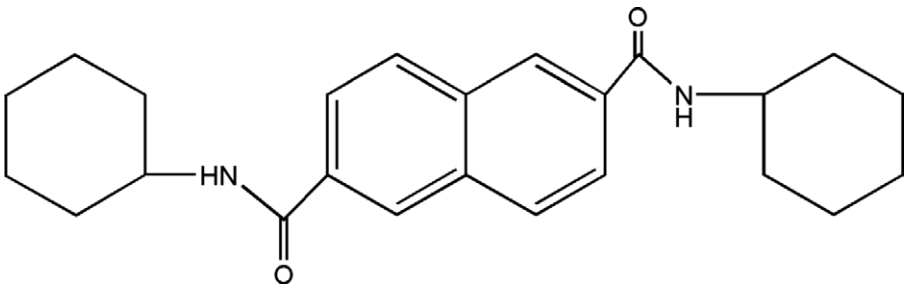

Figure 1 Chemical structure of *N,N′*-Dicyclohexyl-2,6-naphthalenedicarboxamide.

quickly cooling to different temperature from the melt.[38] In other experiments, Li et al. confirmed that DSC crystallization and compression molding processes produced similar amounts of β-iPP higher than what was produced in injection molding.[39] The authored attributed it to lower crystallization temperature and shorter crystallization time in the injection molding process.

TMB-5 is a kind of commercial β type nucleating agent of iPP in local market. In the process of melt mixing, TMB-5 dissolves in the molten polymer and recrystallizes from the melt, before iPP crystallization.[40] In our previous studies, it is shown that diverse structures can develop in the presence of TMB-5, depending on the concentration of the nucleating agent. Microscopy revealed the following characteristic morphologies: (i) β-hedrites in early stage and quasi-spherulites later at "subcritical" concentration (0.01%); (ii) development of microcrystalline clusters at "critical" concentration (0.05–0.1%) and (iii) formation of a transcrystalline layer on the crystal surface of the nucleating agent at "supercritical" concentrations (0.3–1%).

Recently, we discovered iPP/TMB-5 blends could produce high amount of β-iPP even near room temperature, which is advantageous in industry production. By comparisons of quenching with full crystallization, the microstructure and thermal behaviors were examined. WAXD and DSC were utilized to determine the amount of β-iPP and thermal behavior of the samples respectively. The morphological comparisons were displayed by POM and SEM, which will help explain WAXD and DSC results.

EXPERIMENTAL

Materials

The matrix polymer used in this wok was commercial grade PP2401, with melt flow index of 2.5g/10min, $M_w = 4.4 \times 10^5$ g/mol, and melting temperature of 165°C, produced by Yanshan Petroleum and Chemical Corp., China. TMB-5 is a commercialized β-type nucleating agent for iPP, supplied by Shanxi Provincial Institute of Chemical Industry, with melting point of 197°C. Unfortunately, we are not aware of the corresponding work about chemical structure and crystal information of TMB-5 on basis of the relevant patent. As far as we know, it is an aromatic amide derivative with similar chemical structures to some aromatic amine β-nucleating agents, such as N,N′-Dicyclohexyl-2,6-naphthalenedicarboxamide (NJS) of structure (Fig. 1).

Sample preparation

iPP/TMB-5 blends were produced at 190°C for 10 min, with a rotor speed of 60 rpm, using a Torque Rheometer RM-200A, manufactured by Harbin HAPRO Electrical Technology TMB-5 proportion in the blends was 0.01, 0.05, 0.1, 0.3, and 0.6% by weight.

For WAXD and POM measurements, samples were prepared in the film form. The samples in irregular shape piece form were placed between two pieces of aluminum foil. This sandwich was then transferred to a hot press. (The temperature of the press was adjusted to 230°C beforehand.) Pressure was then given for 5 min to obtain the desired film thickness. Two different thermal treatments were applied. The first thermal history, labeled S, consisted of a slow cooling (about 3°C/min) from the molten state down to room temperature, at the inherent cooling rate of the press, after the power was switched off. The second one, named F, applied a fast quench by transferring immediately to another press whose temperature was set at 30°C.

Physical properties

For optical microscopy observation, a Nikon Type 104 optical microscope was used in this study. The optical microscope was equipped with cross-polarizer, with a JVC color video camera incorporated. The film of sample was inserted between two microscope cover glasses.

XRD experiments were conducted with a Rigaku X-ray Diffractometer D/max-2500 (CuKa, $\lambda = 0.154$ nm, 40 kV, 200 mA, reflection mode). The experiments were performed with a 2θ range of 10–30°, at a scanning rate of 6°C/min and a scanning step of 0.02°.

The relative amount of different crystal forms present in these samples was measured from the

X-ray diffraction profiles. In iPP XRD profiles, (110) at $2\theta = 14.1°$, (040) at 16.9°, (130) at 18.5° are the principal reflections of the α-form of iPP while (300) at about 15.9° is the principal reflection of the β-form. They are considered as the characteristic peaks for α-form and β-form respectively. The relative content of β-form, K_β, can be evaluated in the form of the Turner-Jones criterion as follows:[41]

$$K_\beta = \frac{A_{\beta(300)}}{A_{\alpha(110)} + A_{\alpha(040)} + A_{\alpha(130)} + A_{\beta(300)}} \quad (1)$$

where $A_{\beta(300)}$ represents the area of the (300) reflection peak; $A_{\alpha(110)}$, $A_{\alpha(040)}$, and $A_{\alpha(130)}$ represent the areas of the (110), (040), (130) reflection peaks respectively. The overall crystallinity is calculated by

$$X_c = \frac{\sum A_{\text{crystalline}}}{\sum A_{\text{crystalline}} + \sum A_{\text{amorphous}}} \times 100\% \quad (2)$$

$$\sum A_{\text{crystalline}} = A_{\beta(300)} + A_{\alpha(110)} + A_{\alpha(040)} + A_{\alpha(130)} \quad (3)$$

where $A_{\text{crystalline}}$ and $A_{\text{amorphous}}$ are the fitted areas of crystalline and amorphous, respectively.

In this work, the peak intensities of XRD profiles were calculated by a curve-fitting soft by using the mixed function of Gauss and Lorenz. Before analysis, the scattering of air and the empty sample holder was subtracted.

Thermal analysis of samples was performed using Q2900 calorimeter (Thermal Analysis Instruments). All tests were performed in a nitrogen atmosphere with a sample about 2–3 mg. All samples were firstly heated to 230°C at 10°C/min (first heating) and kept for 5 min to eliminate prior thermal history. The specimen was subsequently cooled down to 80°C at a cooling rate of 10°C/min and then heated to 200°C at 10°C/min (second heating).

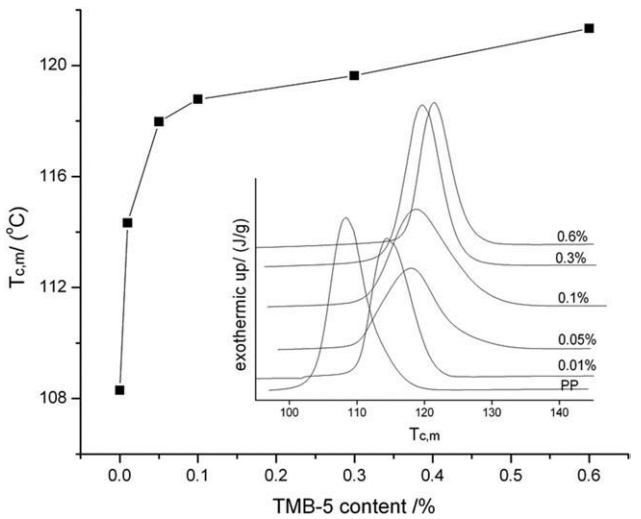

Figure 2 Crystallization temperature as a function of concentration of TMB-5. The inset is DSC scans in a cooling for samples containing different concentration of TMB-5.

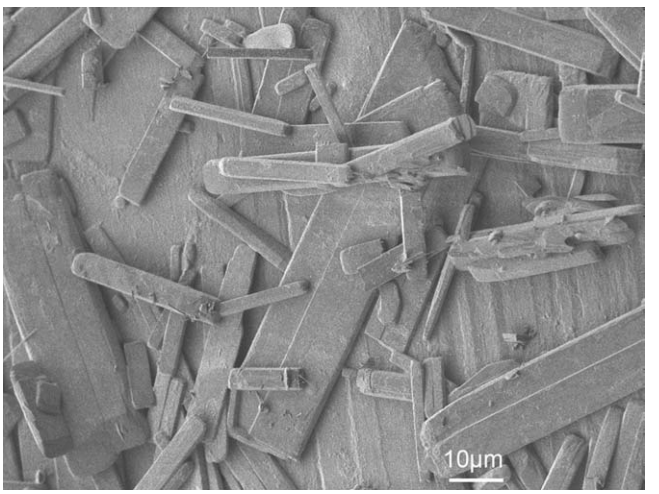

Figure 3 SEM image of TMB-5. Magnification: ×1000.

The temperature-modulated DSC (TM-DSC) melting curves of the quenched samples were recorded with a DSC Q2000 V23.12 Build 103 instrument at scanning rate 2°C/min, modulating ±0.32°C every 60s.

Field emission scanning electron microscopy (FESEM) was performed on a JEOL model JSM-7401 apparatus with an operating voltage of 1.0 kV to investigate the morphology the film. For the purpose of contrasting the crystalline morphology, permanganic etching was used as described by Olley et al.[42] The samples were coated with gold using ETD-200 SEM coating system (Beijing Elaborate Technology Development) operating at 5 mA for 5 min.

RESULTS AND DISCUSSION

Nucleating efficiency of TMB-5

Crystallization temperature is usually adopted to judge when nucleating agent is helpful in promoting crystallization. Figure 2 shows the crystallization curves of iPP/TMB-5 with different TMB-5 content. For pure iPP and TMB-5 nucleated iPP, single exothermic peak is observed. It is clear that the crystallization temperature increases sharply with TMB-5 percentage initially and grows gradually with further addition, indicating that the TMB-5 concentration should surpass a critical concentration 0.05% to function effectively as nucleating agent. Accordingly, 0.01 and 0.3% are referred to sub- and supercritical concentrations of this nucleating agent.[35] In our previous articles, dependence of morphology and crystal structure on dispersion state were reported. Figure 3 shows the bulk shape of nucleating agent. At supercritical contents, the over loaded TMB-5 may aggregate in the form of ruler shape similar to its bulk shape in iPP matrix. The aggregated TMB-5s

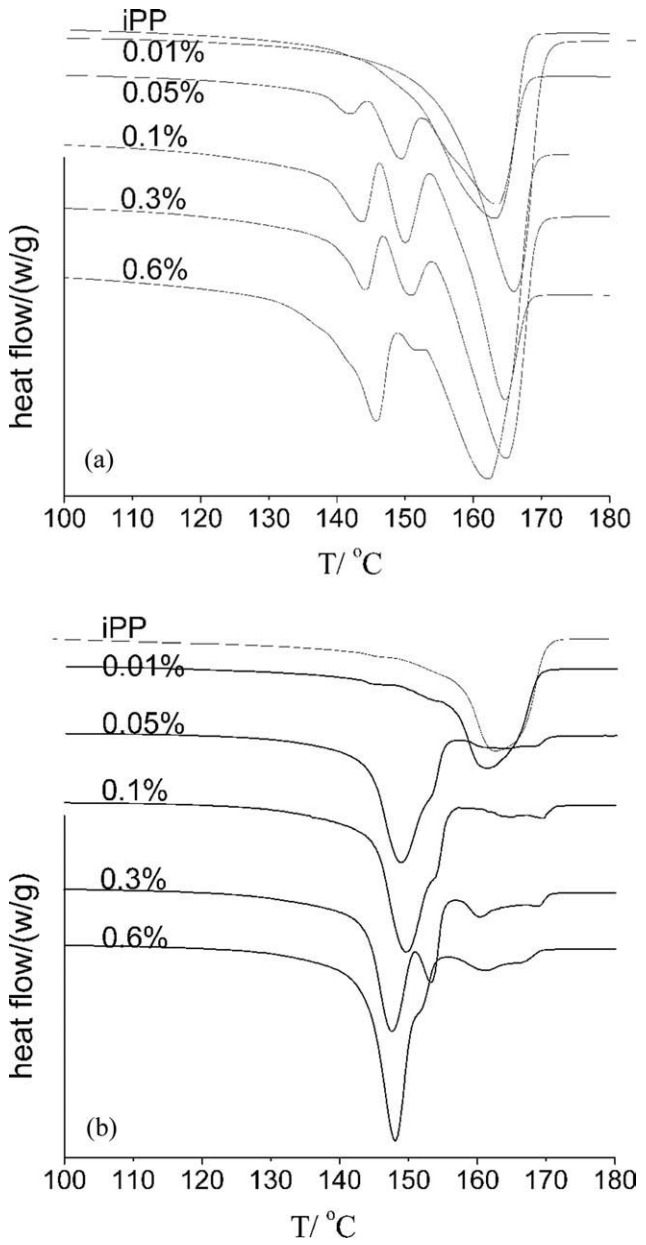

Figure 4 DSC heating thermograms of pure iPP and β-nucleated iPP with various TMB-5 concentrations as indicated. (a) First heating scans of original samples. (b) Second heating scans of crystallized samples.

have lower nucleating ability due to the reduced specific surface area.

The crystal stability of original and DSC crystallized samples

Figure 4(a) shows the DSC thermograms measured during the first heating of the original sample which was prepared in a torque rheometer and then quenched in the air. Figure 4(b) shows the melting curves measured during the second scanning. These curves clearly show the melting characteristics of β-iPP and the effect of thermal history on the samples. The samples exhibit simultaneous melting and recrystallization phenomenon while heating, particularly in the first heating scan. The phase transformation from metastable β-form to stable α-form occurs only by recrystallization during the heating procedure. This behavior is essentially due to the thermodynamic instability of the β-form. The significance of the present study lies in its evaluation of the phase stability and phase transformation behavior under different thermal histories.

When the samples were subjected to the first heating, the thermograms of β-nucleated samples exhibit double peaks between 140 and 150°C and single peak around 160–165°C which belong to the melting

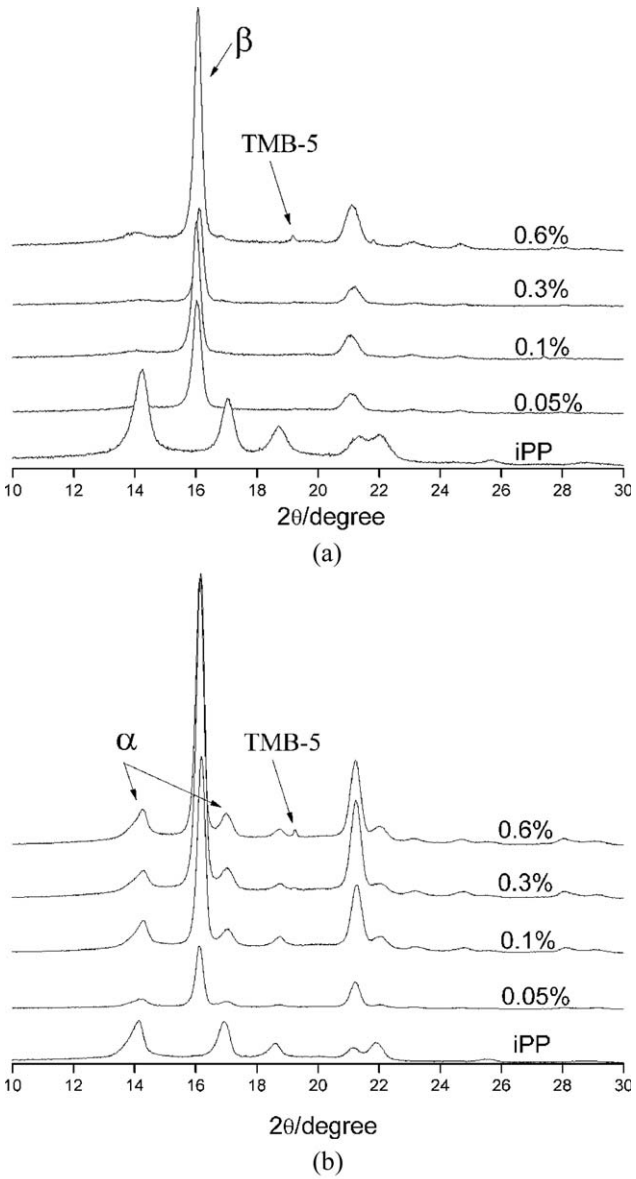

Figure 5 XRD patterns of iPP nucleated with TMB-5. (a) Isothermal crystallization at Tc = 30°C for 10 min; (b) non-isothermal crystallization at $V_{cooling}$ = 3°C/min.

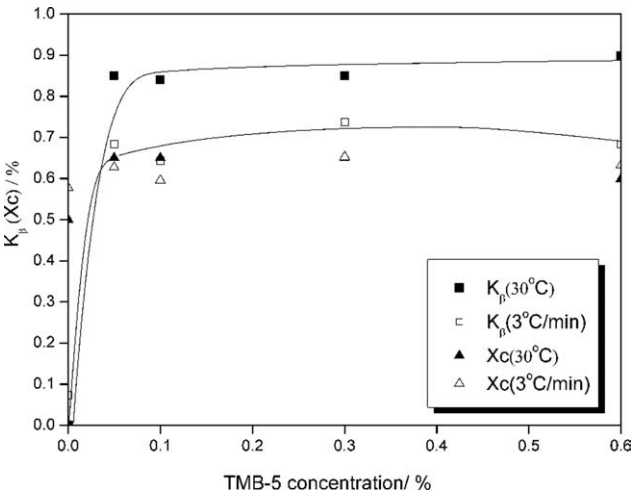

Figure 6 Crystallinity and relative β content (by XRD) of samples in Figure 5.

of the β-form and α-form respectively. According to Varga,[43] the peak duplication is a result of the recrystallization superimposed on melting. The multiple peaks of β-form are attributed to recrystallization-remelting of less stable β-form transformation into stable β′-form. When TMB-5 percentage is increased, the ββ′ transformation is less remarkable, indicating the perfection of crystal is enhanced.

Figure 4(b) shows the second heating thermograms measured from the samples crystallized in DSC. In the second scanning, multiple endotherms are replaced by mainly β-form melting peak. The results are consistent with other literature.[44] The crystals were fully stabled by the recrystallization process and proved again that since the concentration 0.05%, nucleating agent is effective as β form nucleating agent.

The microstructure and thermal behaviors of fast and slow crystallized samples

We have acknowledged that the efficiency of β-form nucleating agents was exerted most under special crystallization conditions in the previous study.[40,45] Because of the occurrence of recrystallization in heating scans of DSC, the microstructures of these samples were investigated by X-ray diffraction under room temperature. The samples were (F) fast and (S) slowly cooled sample films respectively. The XRD patterns are illustrated in Figure 5. According to eqs. (1)–(3), the relative proportion of β-form and total crystallinity degree were calculated. Figure 6 shows that in both thermal treatments nucleating agent is efficient in promoting β-form iPP formation the concentration arrives at 0.05%. Fast cooled samples have higher K_β values (0.85–0.90), indicating that fast cooling is favorable for creating high β content in iPP/TMB-5 system. The β-form content does not increase consistently. The dependence of the K_β values on the concentration of nucleating agents had been investigated by several researchers, and the similar trend was observed.[23,35] Su et al. thought that the result attributed to the change of dispersibility of β-nucleating agents in iPP matrix, which had been confirmed by POM in their article.[23] The over loaded of TMB-5s (0.3–0.6%) of TMB-5 leads to small increase of β-form content. When the content is 0.6%, TMB-5 typical peak can be observed in XRD patterns, meaning compatibility between polymer

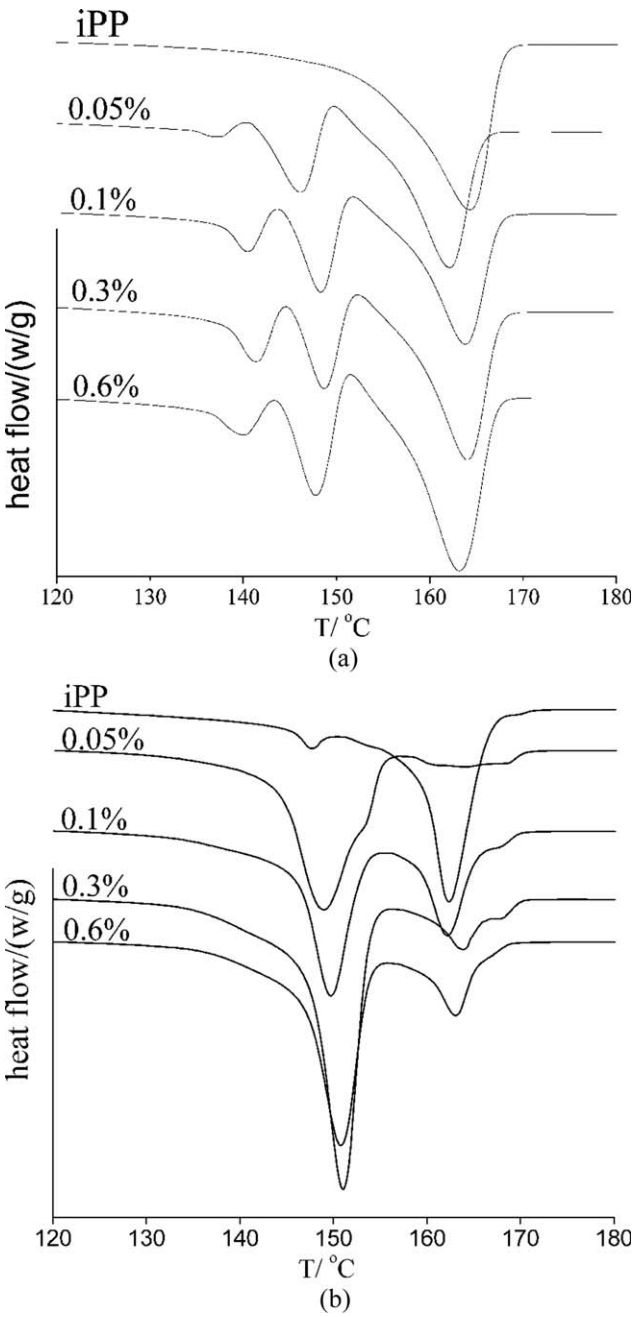

Figure 7 DSC heating thermograms of pure iPP and β-nucleated iPP with various TMB-5 concentrations as indicated. (a) Tc = 30°C. (b) $V_{cooling}$ = 3°C/min.

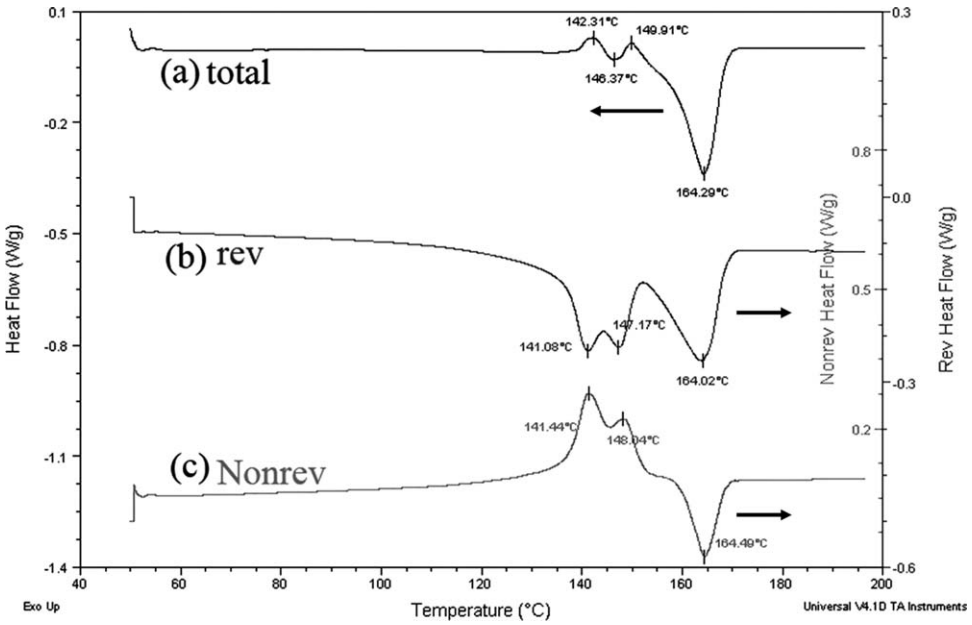

Figure 8 TM-DSC curves of β-nucleated samples containing 0.3% TMB-5. The samples were quenched at 30°C.

matrix and nucleator becomes poor and the latter may separate from the matrix which will be proved in the morphological observations in the next discussion part.

When the fast and slow crystallized samples were heated, we observed thermal behaviors of Figure 7 similar to Figure 4. Incorporating TMB-5 to iPP leads to the increased melting temperature of the β-iPP although the increasing trend is not obvious at super-concentrations (0.3–0.6%). The comparison between the β fraction of crystals obtained from the DSC results (Fig. 7) and the amount of the β phase

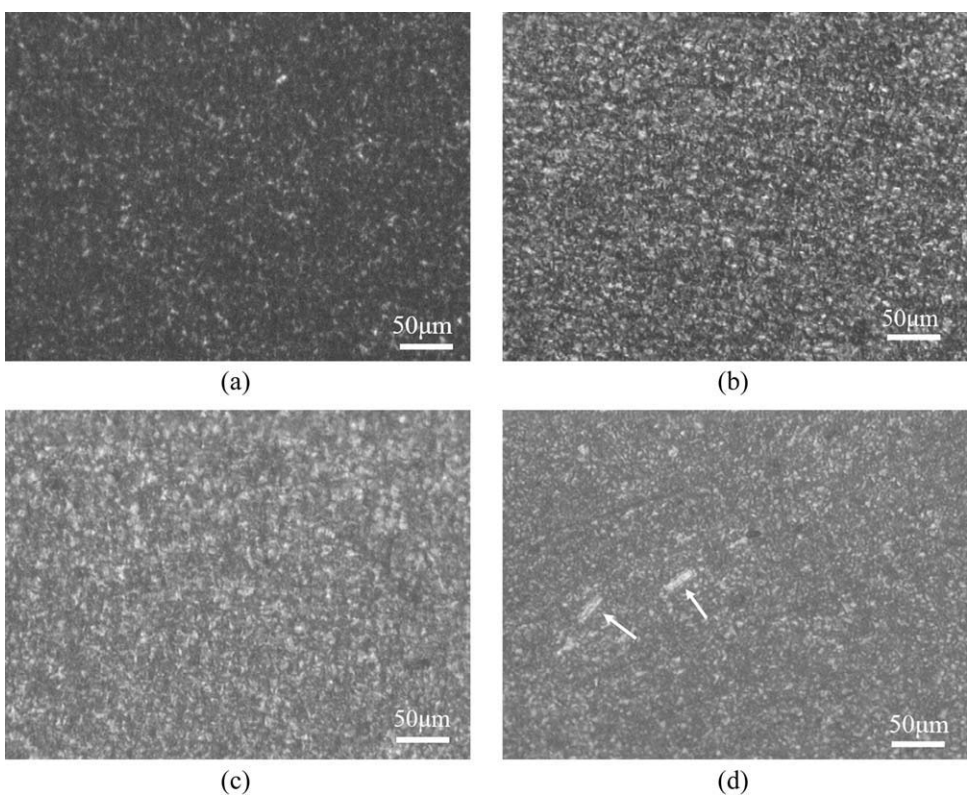

Figure 9 Polarized optical micrographs of iPP nucleated with TMB-5 under Tc = 30°C. TMB-5 concentration: (a) PP; (b) 0.05%; (c) 0.3%; (d) 0.6%.

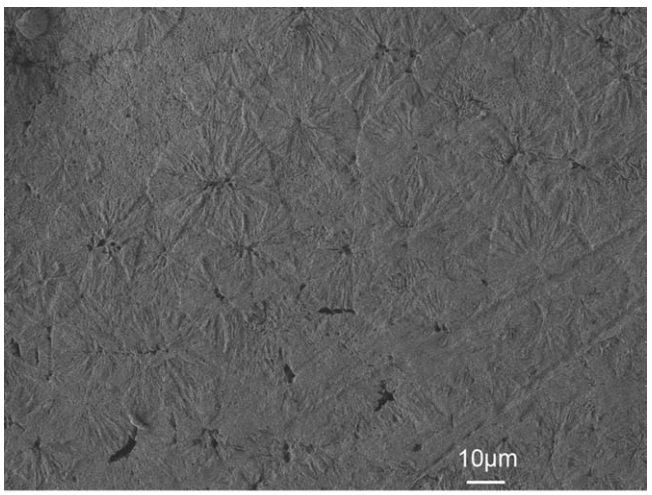

(a)

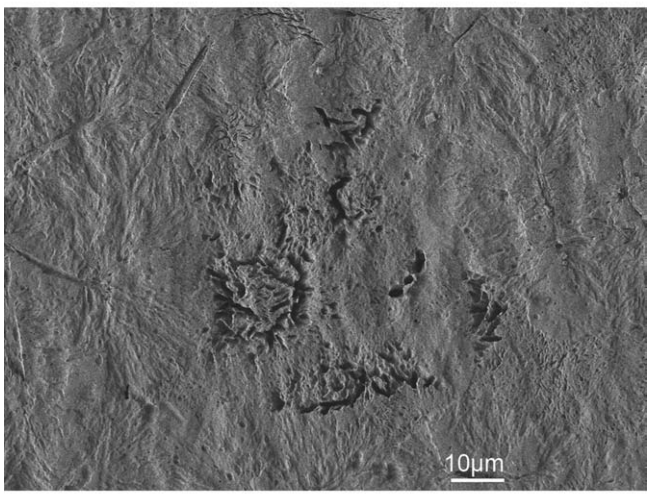

(b)

Figure 10 SEM images of iPP nucleated with TMB-5 under Tc= 30°C. TMB-5 concentration: (a) 0.05%; (b) 0.3%. Magnification: (a) ×700; (b) ×1000.

in the material calculated from the X-ray diffraction (Fig. 6) demonstrates that the existence of a β→α transition considerably increases the fraction of monoclinic crystals that melt, thus increasing the area of α-form endotherm.

The above mentioned processes reflected in the total heat flow recorded during heating (Fig. 8, curve a) can be partly separated by using the TM-DSC technique. The total heat flow has a reversible and an irreversible component. The partial melting of the β-phase is a reversible process with peak temperatures of 141.08°C and 147.17°C which are attributed to the β crystallites with different lamellar thicknesses (Fig. 8, curve b). On the contrary, the exothermic β-recrystallization is an irreversible process with peak temperatures of 141.44°C and 148.04°C which correspond to ββ′ and βα′ recrystallization, respectively (Fig. 8, curve c). It is well discernible in Figure 8 that the temperature lag (0.36°C) between the reversible melting of β-phase and the irreversible ββ′-recrystallization is smaller than that between β′-melting and β′α-recrystallization (0.87°C). Melting of the α-phase contains both reversible and irreversible components.

Spherulitic morphologies of fast and slow cooled samples

The size and perfect degree are close related with crystallization condition and influence directly the properties and application field of materials. POM is a visual method for observing the morphology of different crystals and it is employed in the present study. Figure 9 shows us the crystal morphologies of fast cooled samples. According to Figure 6, the β-nucleated samples have 85–90% of β-iPP. So the tiny crystals in Figure 8(b–d) belong to β-form crystals. The crystals are so fine that we can't figure out the individual crystal morphology. The aggregation of TMB-5 is evident in Figure 9(d), in which "ruler-liked" TMB-5 is found (the white arrows).

Due to small size, the morphological difference is not prominent among the quenching samples. SEM images provide more magnified pictures of these tiny crystals. Figure 10(a) shows spherulite morphology of iPP nucleated with 0.05% TMB-5 when quenched at 30°C. The hollows in the center of β spherulites are the etched TMB-5 particles, proving that dispersed TMB-5 particles induced β nucleation. In this condition β crystal is typical quasi-spherulite with radial structure and the diameter of β spherulite is about 20 μm.

For iPP nucleated with 0.3% TMB-5 [Fig. 10(b)] under quenching conditions, TMB-5s induces β-modification as soon as they recrystallize from the iPP matrix. The time lag between TMB-5 aggregation and iPP crystallization is so short that only very short needles (length around 10 μm) can be formed during TMB-5 recrystallization. The needles and amorphous phase were etched by peroxide solution and left the imprints on the iPP film. The crystals growing perpendicular to the lateral of needle are not well developed. Radial growth of β-spherulites can be observed on the tip of needles.

In Figure 11, we observed distinct morphologies of pure and nucleated iPP crystals when cooled at 3°C/min. Due to different birefringences, α- and β-crystallite morphologies can be easily separated. The pure iPP is mainly made of α-crystals. The proportion of β-crystals increases with increasing TMB-5 concentration until crystal boundaries are hardly observed [Fig. 11(c–d)].

Due to high density of spherulites, the details of crystal morphology are shown by virtue of SEM images (Fig. 12). In the critical concentration sample (0.05%), TMB-5 recrystallizes from the matrix in the

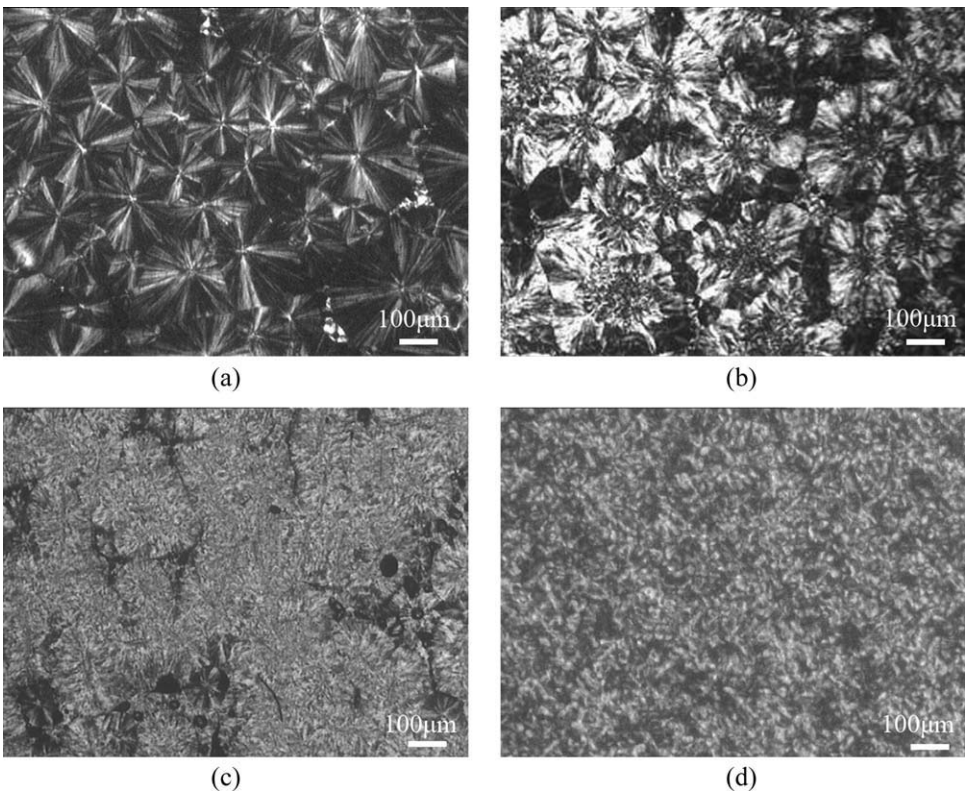

Figure 11 Polarized optical micrographs of iPP nucleated with TMB-5 at $V_{cooling} = 3°C$ /min. TMB-5 concentration: (a) PP; (b) 0.05%; (c) 0.3%; (d) 0.6%.

form of dendritic structure, which is distinctly different from Figure 10(a). Under slow cooling condition, the dendritic structure could fully develop and the radius even extends to 50 μm. The surface of these dendrites hosts a large number of active sites tailored for the nucleation of β-iPP, which present a cluster of microcrystallites.

For supercritical concentration sample (0.3%), under slow cooling condition, the nucleating agent can aggregate into longer ruler shape as long as tens of microns. The bright β spherulites grew in the lateral direction so that a columnar layer, presumed sort of transcrystalline region (TC), was developed on the needle surface. Figure 12(b) is consistent with the POM results. The white arrows indicate chain-folded lamellae of the β-phase standing perpendicular on TMB-5 lateral surface. Part of the TMB-5 ruler has been chemically etched. α- and β-spherulites

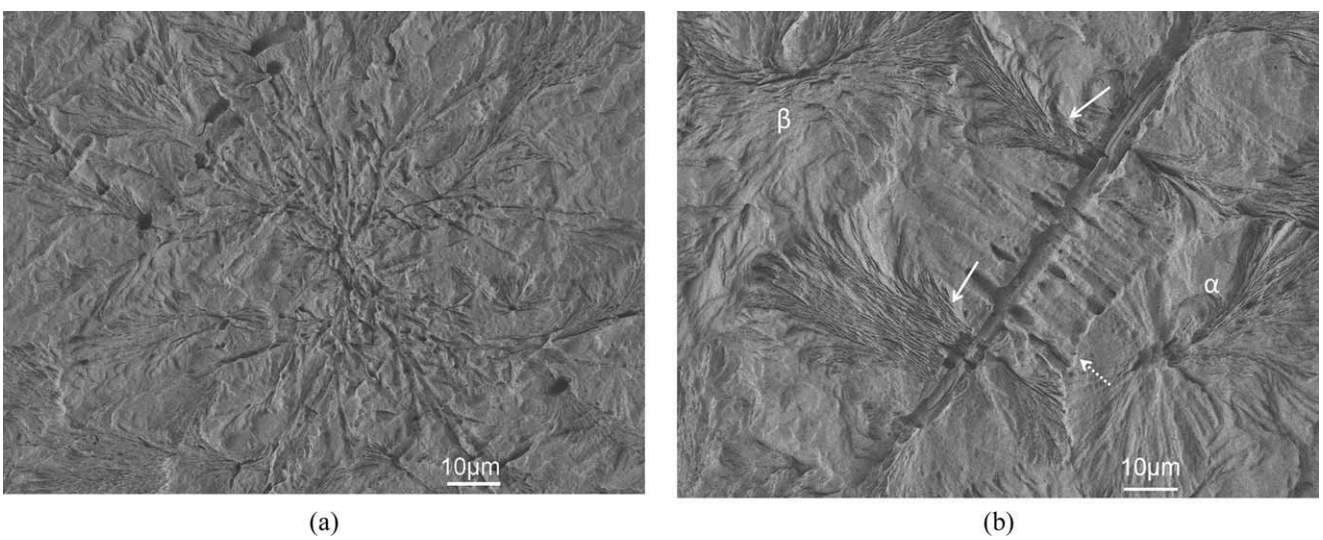

Figure 12 SEM images of iPP nucleated with TMB-5 at $V_{cooling} = 3°C/min$. TMB-5 concentration: (a) 0.05%; (b) 0.3%. Magnification: ×1000.

grow around the β-transcrystalline. The crystalline on the up-left corner belongs to β-spherulite due to its bundle structure. The shape of the boundary between the α-spherulites and β-transcrystalline is particularly conspicuous as the dotted arrow indicates. The boundary line between the β-transcrystalline and the α-spherulite was ellipsoidal. Because of the greater growth rate of the β-form with regard to the α-form, the former crystal developed in the shape of transcrystalline which would lead a bulk α spherulite to develop in a teardrop shape.[46]

CONCLUSIONS

TMB-5 has been proved to be highly efficient nucleating agent for βiPP. The effects of fast and slow crystallization on the microstructure and thermal stability were studied in this article. Fast cooling is favorable for β-modification than that of slow crystallization. iPP/TMB-5 blends could form high amount of β-iPP even at temperature near room temperature, which is of significance in real processing.

However, imperfect crystals were formed and easily transformed into ββ′ or βα′ during this fast crystallization process. With increasing TMB-5 concentration, the thickness of lamellar and the stability of crystal were increased.

POM and SEM images show that under quenching conditions, the crystals are small and undeveloped. During slow cooling, the crystal could develop more fully and present various morphologies with TMB-5 concentration.

References

1. Padden, F. J.; Keith, H. D. J Appl Phys 1959, 30, 1479.
2. Varga, J. J Mater Sci 1992, 27, 2557.
3. Lotz, B.; Wittmann, J. C.; Lovinger, A. J. Polymer 1996, 37, 4979.
4. Meille, S. V.; Brückner, S.; Porzio, W. Macromolecules 1990, 23, 4114.
5. Lotz, B.; Fillon, B.; Thierry, A.; Wittmann, J. C. Polym Bull 1991, 25, 101.
6. Lotz, B. J Macromol Sci Part B 2002, 41, 685.
7. Grein, G. Adv Polym Sci 2005, 188, 43.
8. Čermák, R.; Obadal, M.; Ponížil, P.; Polášková, M.; Stoklasa, K.; Hečková, J. Eur Polym J 2006, 42, 2185.
9. Li, J. X.; Cheung, W. L. Polymer 1998, 39, 6935.
10. Lezak, E.; Bartczak, Z.; Galeski, A. Polymer 2006, 47, 8562.
11. Shangguan, Y. A.; Song, Y. H.; Peng, M.; Li, B. P.; Zheng, Q. Eur Polym J 2005, 41, 1766.
12. Yuan, Y. P.; Chen, B.; Zhang, X. Q. Polymer 2007, 8, 5480.
13. Kotek, J.; Raab, M.; Baldrian, J.; Grellmann, W. J Appl Polym Sci 2002, 85, 1174.
14. Zhao, S.; Cai, Z.; Xin, Z. Polymer 2008, 49, 2745.
15. Li, X. J.; Hu, K. L.; Ji, M. R.; Huang, Y. L.; Zhou, G. E. J Appl Polym Sci 2002, 86, 633.
16. Mohammadian-Gezaz, S.; Ghasemi, I.; Azizi, H.; Karrabi, M. Iranian Polym J 2006, 15, 637.
17. Pawlak, A.; Piorkowska, E. Colloid Polym Sci 2001, 279, 939.
18. Xu, L.; Xu, K.; Chen, D.; Zheng, Q.; Liu, F.; Chen, M. J Therm Anal Calorim 2009, 96, 733.
19. Yuan, Q.; Jiang, W.; An, L.; Misra, R. D. K. Mat Sci Eng A: Struct 2006, 415, 297.
20. Yamaguchi, M.; Fukui, T.; Okamoto, K.; Sasaki, S.; Uchiyama, Y.; Ueoka, C. Polymer 2009, 50, 1497.
21. Yi, Q. F.; Wen, X. J.; Dong, J. Y.; Han, C. C. Polymer 2008, 49, 5053.
22. Shi, G. Y.; Huang, B.; Cao, Y. H.; He, Z. hQ.; Han, Z. W. Makromol Chem 1986, 187, 643.
23. Su, Z.; Dong, M.; Guo, Z.; Yu, J. Macromolecules 2007, 40, 4217.
24. Nagasawa, S.; Fujimori, A.; Masuko, T.; Iguchi, M. Polymer 2005, 46, 5241.
25. Zheng, Q.; Shangguan, Y.; Yan, S. K.; Song, Y. H.; Peng, M.; Zhang, Q. B. Polymer 2005, 46, 3163.
26. Su, Z. Q.; Wang, H. Y.; Dong, J. Y.; Zhang, X. Q.; Dong, X.; Zhao, Y.; Yu, J.; Han, C. C.; Xu, D. F.; Wang, D. J. Polymer 2007, 870.
27. Li, H. H.; Jiang, S. D.; Wang, J. J.; Wang, D. J.; Yan, S. K. Macromolecules 2003, 36, 2802.
28. Zhang, C. G.; Hu, H. Q.; Wang, D. J.; Yan, S. K.; Han, C. C. Polymer 2005, 46, 8157.
29. Kawai, T.; Iijima, R.; Yamamoto, Y.; Kimura, T. Polymer 2002, 43, 7301.
30. Song, B.; Wang, Y.; Bai, H.; Liu, L. J Therm Anal Calorim 2010, 99, 563.
31. Hoffman, J. D.; Miller, R. L. Polymer 1997, 38, 3151.
32. Zhu, P. W.; Tung, J.; Philips, A.; Edward, G. Macromolecules 2006, 39, 1821.
33. Hou, W. M.; Liu, G.; Zhou, J. J.; Gao, X.; Li, Y.; Li, L.; Zheng, S.; Xin, Z.; Zhao, L. Q. Colloid Polym Sci 2006, 285, 11.
34. Obadal, M.; Čermák, R.; Raab, M.; Verney, V.; Commereuc, S. Polym Degrad Stab 2005, 88, 532.
35. Varga, J.; Menyhárd, A. Macromolecules 2007, 40, 2422.
36. Ščudla, J.; Raab, M.; Eichhorn, K. J.; Strachota, A. Polymer 2003, 44, 4655.
37. Bruckner, S.; Meille, S. V.; Petraccone, V.; Pirozzi, B. Prog Polym Sci 1991, 16, 361.
38. Gomez, M. A.; Tanaka, H.; Tonelli, A. E. Polymer 1987, 28, 2227.
39. Li, J. X.; Cheung, W. L. J Vinyl Additive Technol 1997, 3, 151.
40. Dong, M.; Guo, Z. X.; Yu, J.; Su, Z. Q. J Polym Sci Part B: Polym Phys 2009, 47, 314.
41. Jones, A. T.; Aizlewood, J. M.; Beckett, D. R. Makromol Chem 1964, 75, 134.
42. Olley, R. H.; Hogue, A. M.; Bassett, D. C.; Thomson, J. J. J Polym Sci Part B: Polym Phys 1979, 17, 627.
43. Varga, J.; Mudra, I.; Ehrenstein, G. W. J Therm Anal Cal 1999, 56, 1047.
44. Varga, J.; Mudra, I.; Ehrenstein, G. W. J Appl Polym Sci 1999, 74, 2357.
45. Dong, M.; Guo, Z. X.; Yu, J.; Su, Z. Q. J Polym Sci Part B: Polym Phys 2008, 46, 1725.
46. Wua, C. M.; Chena, M.; Karger-Kocsisb, J. Polymer 1999, 40, 4195.